

Environmental Science Nano

Accepted Manuscript

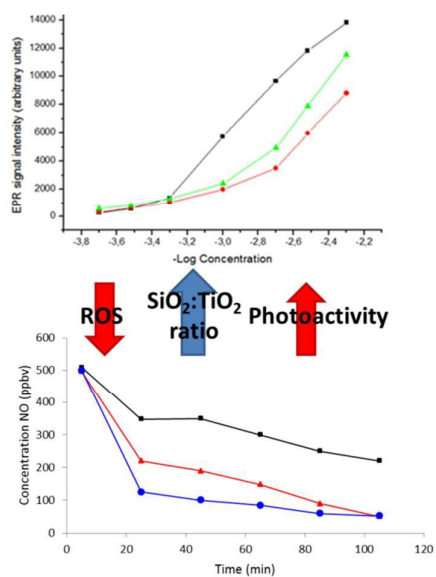


This is an *Accepted Manuscript*, which has been through the Royal Society of Chemistry peer review process and has been accepted for publication.

Accepted Manuscripts are published online shortly after acceptance, before technical editing, formatting and proof reading. Using this free service, authors can make their results available to the community, in citable form, before we publish the edited article. We will replace this *Accepted Manuscript* with the edited and formatted *Advance Article* as soon as it is available.

You can find more information about *Accepted Manuscripts* in the [Information for Authors](#).

Please note that technical editing may introduce minor changes to the text and/or graphics, which may alter content. The journal's standard [Terms & Conditions](#) and the [Ethical guidelines](#) still apply. In no event shall the Royal Society of Chemistry be held responsible for any errors or omissions in this *Accepted Manuscript* or any consequences arising from the use of any information it contains.



Silica matrix encapsulation can control potential health risk associated to ROS production, but improves as well the photocatalytic properties of nano TiO₂.

Silica matrix encapsulation as a strategy to control ROS production while preserving photoreactivity in nano-TiO₂

Simona Ortelli¹, Craig Poland², Giovanni Baldi³ and Anna Luisa Costa^{1*}

¹ *ISTEC-CNR, Institute of Science and Technology for Ceramics–Italian National Research Council, Via Granarolo 64, I-48018 Faenza (RA), Italy*

² *Institute of Occupational Medicine, Research Avenue North, Riccarton, Edinburgh EH14 4AP, United Kingdom*

³ *Ce.Ri.Col -Centro Ricerche Colorobbia, Colorobbia Consulting s.r.l. (COLOR), Via Pietramarina, 53 I-50053 SOVIGLIANA, Vinci (FI), Italy*

*Corresponding author: Anna Luisa Costa, e-mail: anna.costa@istec.cnr.it, Tel. +39 0564 699718.

Abstract

In this work, the application of a silica coating on TiO₂ nanoparticles (NPs) represented a material design strategy at the purpose of controlling the reactive oxygen species (ROS) production, identified as one of the potentially hazardous effect for this class of materials. The study focused on characterizing redox reactivity as a source of potential adverse cellular oxidative stress and desirable photocatalytic reactivity. The SiO₂-modified TiO₂ systems were produced using a colloidal heterocoagulation method expected to give rise to “matrix encapsulation” and the formation of a mixed structure. To assess the effect of SiO₂ surface engineering on TiO₂ NP redox reactivity, ROS production was measured by electron paramagnetic resonance (EPR) and photocatalytic tests based on NO_x/NO abatement analysis were carried out. The obtained reduction in ROS production associated with an improved photoactivity in the SiO₂-modified samples, by comparison with TiO₂ pristine ones, encouraged the promotion of silica coating as “safer by molecular design” strategy.

Keywords: Titania-Silica; Safety by molecular design; ROS; NO_x abatement.

1. Introduction

Titania is a very well-known and well-researched material because of its stable chemical structure, biocompatibility, and physical, optical, electrical and photocatalytic properties [1-3]. In particular, nano-TiO₂ is the most often-used photocatalyst thanks to its high nanoscale reactivity, easy synthesis, stability under various reaction media, low cost, and band position compatible with the oxidation of many organic compounds [4]. Its photocatalytic properties have been exploited in various environmental applications to remove contaminants from air and water [5]. In recent years,

numerous studies have focused on NO_x abatement by means of photocatalytic TiO₂-based nanomaterials (NMs) [6-10]. NO_x pollution is responsible for well-known environmental problems such as tropospheric ozone production, acid rain, and global warming, and it can affect human health, and the respiratory and immune systems in particular [11]. Its consequently amply-investigated and widely-developed commercial environment- and health-related applications justify an increasingly close attention to safety issues. The great variety of NMs' physicochemical parameters, such as their size, shape, structure, crystallinity and elemental properties, makes investigating their toxic effects a major challenge, however. Some of the paradigms for nanoparticle-mediated toxicity include oxidative stress, inflammation, genetic damage, and the inhibition of cell division and cell death [12-15]. TiO₂ is known as an exogenous source of reactive oxygen species (ROS) that can interact with redox metabolic mechanisms and induce an inflammogenic response. That is why ROS production by NMs is one of the structural alerts to consider when assessing the potential hazards of NMs [16-18]. Changes in the structural and physicochemical properties of nanoparticles (NPs) can lead to changes in their biological activities, which include the generation of ROS, a recognized key risk determinant. Thanks to an increasing understanding of nanotechnological developments and the related occupational health and safety issues, there is a new awareness that safety options should also include "smart" nanoparticle design (i.e. making materials "safer by molecular design" [SbD]) as an effective approach to risk prevention [19]. The development of SbD risk remediation strategies (RRSs) is challenging, but the state-of-the-art objective is to design out risks rather than address them when they occur. These strategies can provide the breakthrough means to control the occupational risks of exposure to NMs. Several studies investigating the structure-activity relationship in NMs suggest useful pathways for the safer design of engineered NMs, including calcination, doping, surface coating, and surface charge modification [20-29]. ROS production has been recognized as one of the key risk determinants in this setting, directly related to the induction of cellular oxidative stress phenomena [30]. Given the direct correlation between surface properties (shell composition, charge, defects, etc.) and NM reactivity, there are several approaches available for modifying the surface of TiO₂ to control its redox reactivity. NP surface engineering and encapsulation with silica has been tested as a strategy for reducing NP toxicity. Soturius, *et al.* reported that applying a SiO₂ coating on ZnO nanorods significantly reduces the strong DNA damage otherwise observed with pure, uncoated ZnO nanorods [31]. Malvindi, *et al.* found that the surface engineering of Fe₃O₄/SiO₂ NPs played a key part in improving particle stability in biological environments, reducing their cytotoxic and genotoxic effects [32]. Ma, *et al.* presented a study on the "safer by design" concept of encapsulating CeO₂ with a nanothin layer of SiO₂ to partially protect against CeO₂-induced pulmonary reactions [33]. Singh, *et al.* confirmed that a layer of silica significantly reduced cellular toxicity judging from the increased cell viability and reduced ROS production during 48 h of culture on magnetite NPs [34].

In the present work, the application of a silica coating on TiO₂ NPs was developed for controlling redox reactivity, affecting both ROS production and the NPs' desirable photocatalytic reactivity, following one of the most promising approach to control and reduce the potential hazard of this class of materials. The coating was applied using a colloidal heterocoagulation method [35-38], exploiting electrostatic interactions between negatively-charged silica NPs and positively-charged titania NPs.

Electron paramagnetic resonance (EPR) was used to evaluate ROS production. Although no single assay can predict NM-related oxidative stress completely [39], the ability of NMs to produce ROS [40,41] was correlated indirectly with their potential adverse bio-effects. The NMs' photocatalytic performance was assessed, including an NO_x/NO abatement analysis (DeNO_x activity) on coated ceramic tiles, to see what effects the silica coating had on the TiO₂'s functional property photoactivity, since preserving a material's performance after applying a given design strategy is mandatory for the promotion and sustainability of an SbD approach.

2. Experimental

2.1 Materials

The following commercial materials were used to prepare the TiO₂/SiO₂ samples: TiO₂ colloidal nanosuspension (TiO₂_6) containing 6 wt% titania, (Colorobbia, Italy) and SiO₂ colloidal nanosuspension (SiO₂_1) Ludox HS-40® containing 40 wt% silica (Grace Davison, USA). Tempone-H hydrochloride (1-hydroxyl-2,2,6,6-tetramethyl-4-oxo-piperidine · HCl), used as a spin trap molecule, was purchased from Enzo Life Sciences.

2.2 Preparation of SiO₂-modified TiO₂ samples

The commercial colloidal nanosuspensions (nanosols) were diluted with water (TiO₂ and SiO₂ nanosols to 3 wt%), and the SiO₂ nanosol was acidified by cationic exchange on resin to obtain a pH of 4 [42]. After this treatment, the titania and silica nanosols were mixed in well-defined ratios (TiO₂:SiO₂ weight ratios 1:3 and 1:5) and ball milled for 24 hours with zirconia spheres (5 mm in diameter), generating samples of TiO₂_18_Sil and TiO₂_19_Sil (TiO₂ content: 10 g/L). TiO₂_37_Sil samples, characterized by a TiO₂:SiO₂ w/w ratio of 1:3 and a TiO₂ content of 2.5 g/L, were prepared in the same way.

2.3 Characterization of colloidal nanosol samples

The hydrodynamic diameter of the samples, dispersed at 0.1g/L in deionized water, was measured with a Zetasizer nano ZSP (model ZEN5600, Malvern Instruments, UK). The hydrodynamic diameter (d_{DLS}) of the NPs was obtained from dynamic light scattering (DLS) data, setting the measurement angle to 173° and the measurement time on automatic. After a 2 min temperature equilibration step, 1 mL of the sample was measured consecutively three times at 25°C and

particle size distributions by intensity were obtained by averaging the three measurements. The zeta potential (ζ -pot) was measured with an electrophoretic light scattering (ELS) method using the Zetasizer nano ZSP. The Smoluchowski approximation was applied to convert the electrophoretic mobility into the zeta potential. The ζ -pot was measured on 700 μL of the sample at 25°C, setting the measurement time, the attenuator position and the applied voltage to automatic. After a 2 min temperature equilibration step, the samples (0.1g/L in deionized water) were measured three times, and the data were obtained by averaging the three measurements.

The pristine and SiO_2 -modified titania samples underwent morphological analysis using the FEI Titan transmission electron microscope (TEM) operating at an acceleration voltage of 300kV. One drop of nanoparticle suspension diluted in deionized water (30 $\mu\text{g/mL}$) was deposited on a film-coated copper grid and characterized.

2.4 Characterization of powder samples

To better characterize the silica-modified titania NP samples, the heterocoagulated nanosols (TiO_2_{18} and TiO_2_{19}) were spray-dried in counterflow with a stream of hot air (at 220°C) through a nozzle 500 μm in diameter (Figure 1). This process could also improve the adhesion of silica NPs on the surface of the TiO_2 NPs. The resulting spray-dried powders contained TiO_2 : SiO_2 w/w ratios of 1:3 and 1:5, and were called $\text{TiO}_2_{21_Sil}$ and $\text{TiO}_2_{22_Sil}$, respectively. The pristine TiO_2 and SiO_2 nanosols were also spray-dried, obtaining the TiO_2_{15} and SiO_2_2 samples. The spray-dried powders were characterized by X-ray diffraction (XRD), the Brunauer-Emmett-Teller (BET) method and ζ -pot analyses. The XRD patterns were obtained on the TiO_2_6 , $\text{TiO}_2_{21_Sil}$ and $\text{TiO}_2_{21_Sil}$ samples using a Bragg-Brentano diffractometer (Bruker D8 Advance, Karlsruhe, Germany) operating in a $\theta/2\theta$ configuration, with an X-Celerator detector LynkEye (10°–80°, 2θ range, 0.02 step size, 1 s per step). Surface area (SA) measurements were obtained with the BET method, using N_2 as the adsorptive gas, in a Sorptly 1750 (Carlo Erba, Italy). The spray-dried powders were dispersed 0.1g/L in deionized water and the ζ -pot was measured by ELS using the Zetasizer nano ZSP, as explained in Section 2.3. Spectrophotometric measurements [43,44] were obtained to assess the band gap energy (E_g) of the different spray-dried powders, using the Lambda 35 (Perkin Elmer) spectrophotometer equipped with the integrating sphere Labsphere RSA-PE-20. The standard Spectralon (Labsphere SRS-99-010) is the reference material for blank tests.

Diffuse reflectance spectra were collected and converted into $F(R)$ using the Kubelka-Munk equation (Eq. 1)

$$F(R) = \frac{(1-R)^2}{2R} \quad \text{Eq. 1}$$

where R is the reflectance collected at any wavelength.

The Tauc relationship was then applied to calculate the band gap energy (Eq. 2)

$$(F(R)hv)^{1/n} = A(hv - E_g) \quad \text{Eq. 2}$$

where h is Planck's constant (6626×10^{-34} J s), A is a proportional constant, ν is the frequency of vibration (s^{-1}), and the value of the exponent n denotes the nature of the electronic transition, the value of which differs for each kind of transition involved; in this case, $n = 2$ was chosen for TiO_2 , indicating indirect allowable electronic transitions. The E_g values were finally obtained by plotting $[F(R)hv]^{1/n}$ vs $h\nu$ (Tauc plot) and extrapolating the intercept between the linear part of the curves and the x axis.

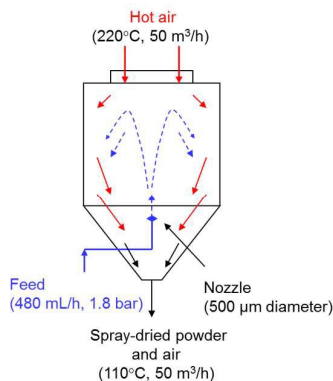


Figure 1. Spray-drying technique applied to the heterocoagulated nanosols.

2.5 EPR analysis

The samples were freshly prepared in Krebs buffer solution (composition: 118.4 mM NaCl, 25mM NaHCO_3 , 11 mM glucose, 4.7 mM KCl, 1.2 mM MgSO_4 , 1.2mM KH_2PO_4 and 2.5 mM CaCl_2 , pH 7.4). A very diluted buffer solution was used for all samples (TiO_2_6 , $\text{TiO}_2_18_Sil$ and $\text{TiO}_2_19_Sil$) to avoid destabilizing the NPs. All the dispersions were sonicated for 15 minutes (US 70; Philip Harris Scientific, Lichfield, UK) before use to obtain more homogeneous samples to analyze. The value of the blank in the presence of HCl 0.01M was subtracted to simulate the pH of the TiO_2 suspensions because the pH is one of the parameters to check during the readings as it affects ROS generation and the stability of the spin trap molecule. All the colloidal samples were diluted to 10 mg/L to prepare the suspensions to analyze. EPR with the spin trap technique was used to monitor ROS formation, and particularly the superoxide radicals ($\text{O}_2^{\bullet-}$) and hydroxyl radicals generated during TiO_2 NP irradiation with a mercury UV lamp. Tempone-H hydrochloride (1-hydroxyl-2,2,6,6-tetramethyl-4-oxo-piperidine \cdot HCl) was used as a spin trap molecule [45]. The spin-trap was dissolved in a 0.01 M EDTA (final concentration 0.1mM) to minimize the autoxidation induced by metal ions. Pyrogallol (320 μM) in Krebs buffer solution was used as a positive control to assess the generation of superoxide radicals during the analysis [46]. The samples were kept at 37°C with the aid of a thermostat, and measurements were taken after 0, 20, 40 and 60 minutes of irradiation with a mercury UV lamp ($\lambda_{\text{max}} = 254$ nm) by drawing 50 μL of sample into a capillary tube (Scientific Laboratory Ltd., Coatbridge, UK) and sealing it with a plug of soft sealing agent

(Cristaseal, VWR International, Lutterworth, UK). The intensity of the EPR peak monitored during the irradiation time and subtracted from the blank value was the parameter used to quantify ROS generation and compare the different compositions of TiO₂ NPs. The EPR spectrometer settings and parameters typical of a standard photochemical experiment were used, i.e. microwave frequency 9.30-9.55 Hz, microwave power 20Mw, modulation frequency 100 KHz, modulation amplitude 1500 Mg, center field 3365 G, sweep width 50 G, sweep time 30 s, and number of passes 1 [47].

2.6 NO_x abatement test

The NO_x abatement test was conducted on pristine (TiO₂_6) and silica-modified (TiO₂_18_Sil and TiO₂_37_Sil) samples. The analyses were performed by applying 5 g of nanosol sample on ceramic tiles (20x20 cm) with a spray-gun. The coated ceramic tiles underwent a heat treatment at 700°C for 1 h, at a heating rate of 350°C/h. The analyses were conducted under controlled conditions, at a temperature of 23 ± 2°C and a relative humidity of 40 ± 2%, under UV irradiation at an intensity of 50 W/m² with an illumination wavelength in the range of 300-400 nm (Osram ULTRA-Vitalux lamp 300 W). The coated ceramic tiles were irradiated from a distance of 20 cm. The lamp was switched on 30 min before starting the test to stabilize the power of its emission spectrum. The analyses were performed by injecting a pollutant gas consisting of dry air, moist air and NO in the measuring system in the presence of the ceramic tiles. Then the concentration of the gases (NO, NO_x and NO₂) was monitored with a chemiluminescent detector (Thermo, model 42i), assessing the NO_x/NO abatement achieved by the TiO₂-based coating on the ceramic tiles.

3. Results and Discussion

3.1 Characterization of colloidal nanosol samples

The main physicochemical characteristics of the nano-TiO₂-based samples are given in Table 1.

The increase in hydrodynamic diameter as a function of the amount of SiO₂ is caused by the steric hindrance of the SiO₂ heterocoagulated on the surface of the TiO₂ [48,49], and by electrostatic destabilization due to the gradual neutralization of the TiO₂ surface charge with the increase in SiO₂ content.

Pristine TiO₂ and SiO₂ NPs were positively and negatively charged, as expected (Table 1). In the silica-modified samples (TiO₂_18_Sil and TiO₂_19_Sil), the decrease in ζ-pot suggests a casual reorganization of the TiO₂ aggregates in the silica matrix, which could indicate that matrix encapsulation structures are obtained.

The TEM micrograph of the commercial TiO₂ sample shown in Figure 2a reveals a primary structure that is very fine, but organized in the form of diffused aggregates, as the DLS data demonstrate. The diameter of the primary NPs is

about 5 nm, corresponding to the crystal lattice shown in the TEM image (Fig. 2b). The structure of the silica nanosol was almost monodispersed, with spherical primary particles having a mean diameter of around 20 nm, as seen in the scanning TEM image (Fig. 2c) and confirmed by the d_{DLS} value. The STEM image (Fig. 2d) also reveals the presence of amorphous SiO_2 particles.

Table 1. Main features of $\text{TiO}_2/\text{SiO}_2$ nanosol samples.

| Sample code | TiO_2 content (g/L) | SiO_2 content (g/L) | d_{DLS} (nm) | ζ -pot (mV) |
|--------------------------|------------------------------|------------------------------|-----------------------|-------------------|
| TiO ₂ _6 | 10 | 0 | 53 ± 0.9 | $+38 \pm 1.8$ |
| TiO ₂ _18_Sil | 10 | 40 | 110 ± 0.9 | $+31 \pm 1.0$ |
| TiO ₂ _19_Sil | 10 | 60 | 577 ± 39 | $+25 \pm 0.1$ |
| TiO ₂ _37_Sil | 2.5 | 10 | 95 ± 0.9 | nd* |
| SiO ₂ _1 | 0 | 10 | 20 ± 0.3 | -42 ± 2.2 |

nd*: not determined

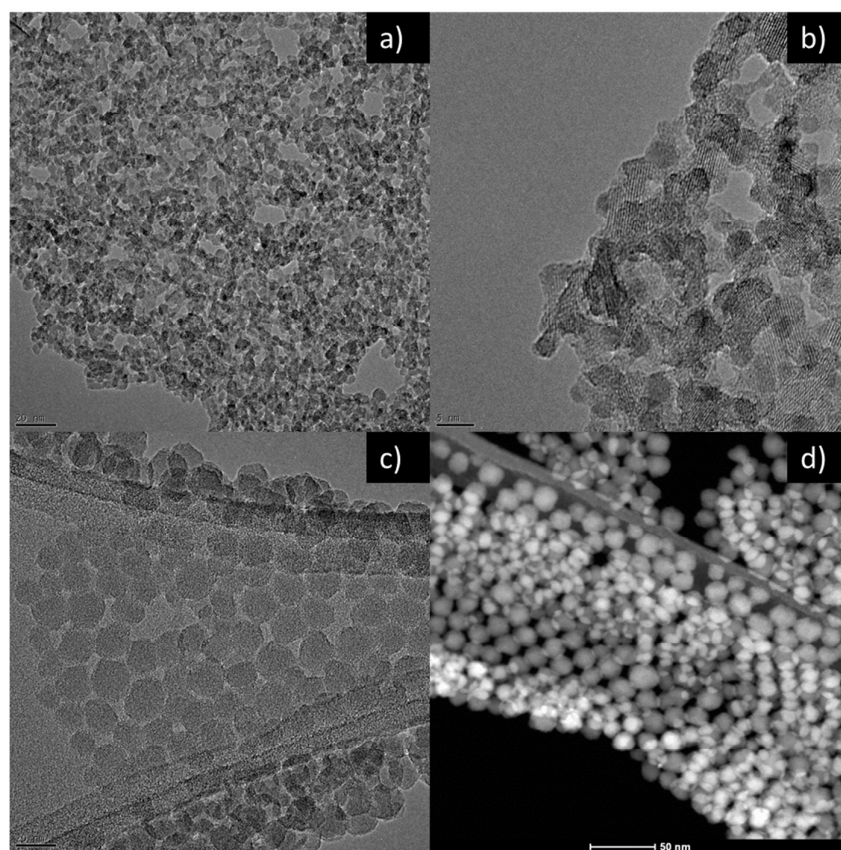


Figure 2. TEM images of commercial nanosol samples: a) and b) TiO_2_6 ; c) and d) SiO_2_1 .

The $\text{TiO}_2_18_{\text{Sil}}$ sample was aggregated with TiO_2 randomly distributed within a silica matrix. This structure was as expected from a matrix encapsulation process based on colloidal heterocoagulation [50,51], as already seen from the ζ -

pot data. The two phases were clearly identified due to the presence of the TiO_2 crystalline phase, as shown in Figure 3a. The presence of aggregates formed of a mixture of nano- TiO_2 and nano- SiO_2 phases is clearly visible in Figure 3b. The TiO_2 _19_Sil sample also showed the expected mixed structure (Fig. 3c and 3d). Given a greater excess of the SiO_2 phase (TiO_2 _19_Sil sample), EDX analysis of the elemental distribution confirmed the presence of a matrix encapsulation structure, where the TiO_2 NPs were surrounded by SiO_2 NPs (Fig. 4).

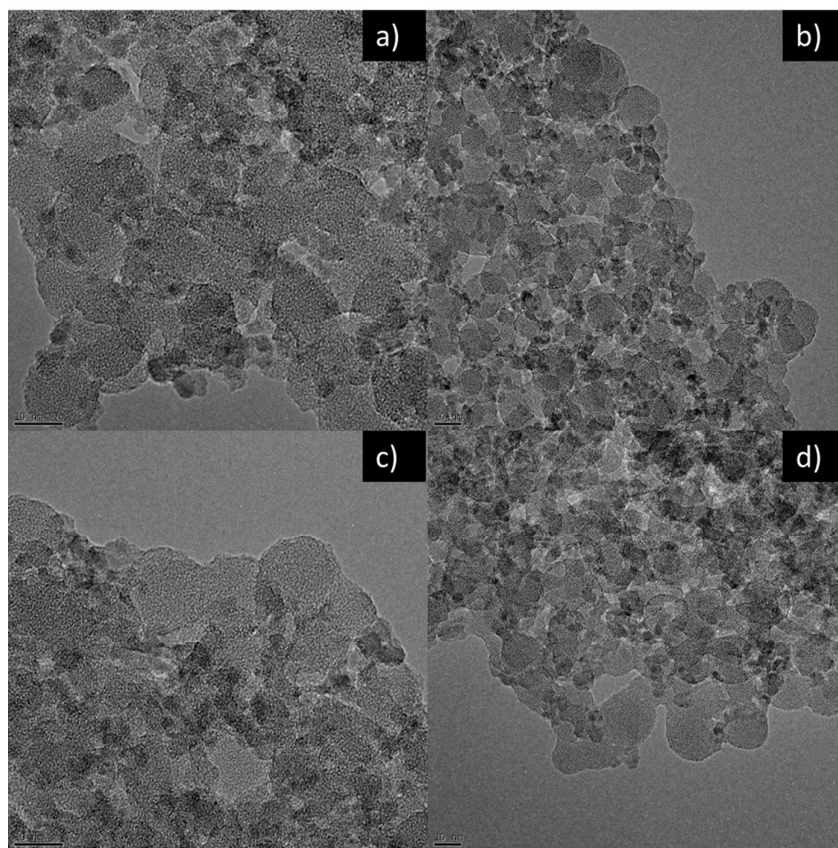


Figure 3. TEM images of SiO_2 -modified TiO_2 nanosol samples: a) and b) TiO_2 _18_Sil; c) and d) TiO_2 _19_Sil.

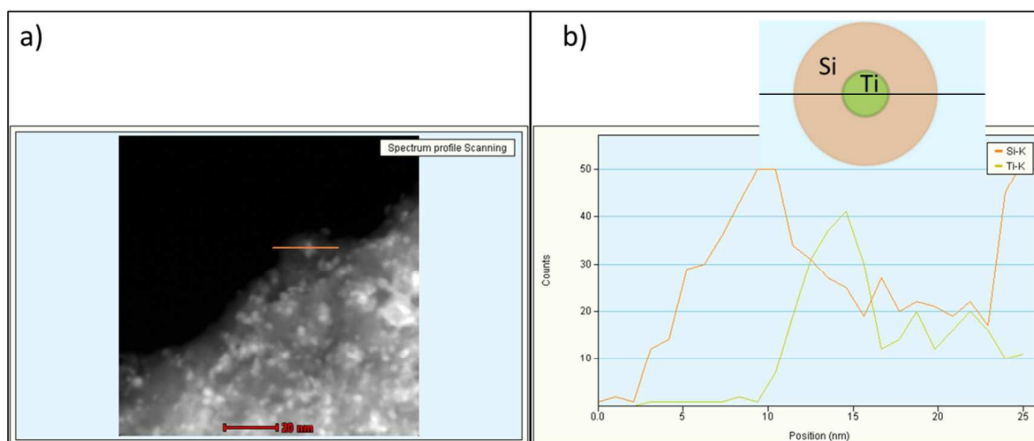


Figure 4. EDX-STEM analysis on the TiO_2 _19_Sil sample: a) sample area analyzed; b) Si and Ti distribution within the selected area confirms the phase gradient represented in the sketch.

3.2 Characterization of powder samples

Figure 4 shows the XRD patterns for the TiO₂_15, TiO₂_21_Sil and TiO₂_22_Sil powder samples. Anatase (JCPDS 21-1272) is predominant in the commercial TiO₂ sample (TiO₂_15), and there are small amounts of brookite (JCPDS 29-1360) and rutile (JCPDS 65-0190). In the silica-modified samples (TiO₂_21_Sil and TiO₂_22_Sil), there is a broad band centered at $2\theta = 22.0$, the characteristic peak for amorphous SiO₂ (JCPDS 29-0085) [52], with an intensity proportional to the amount of silica added. The presence of silica also induced a decrease in the crystallinity of the TiO₂ peaks consistent with the electrostatic interactions occurring between the titania and silica.

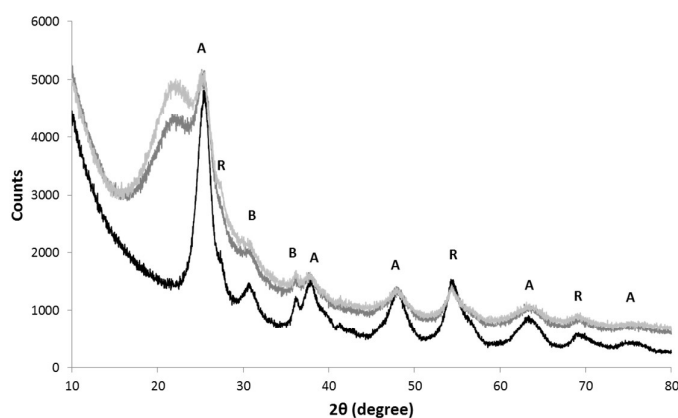


Figure 4. X-ray diffractograms of TiO₂_15 (black), TiO₂_21_Sil (medium gray, TiO₂/SiO₂: 1:3) and TiO₂_22_Sil (light gray, TiO₂/SiO₂: 1:5); (A = anatase; B = brookite; R = rutile).

The surface area of the uncoated and silica-coated TiO₂ powders was higher than 150 m²/g, confirming the preservation of a nanostructured form even after the drying process. Table 2 summarizes the SA data and the ζ -pot of the spray-dried samples. The drop in ζ -pot from the pristine TiO₂ to the silica-coated samples, with a reversing of the positive sign coinciding with the higher silica content, is consistent with a silica encapsulating structure masking the positive sign of the TiO₂ particles towards the negative value of the SiO₂.

The results of the band gap energy (E_g) measurements on the spray-dried powders are shown in Table 2. They are consistent with the reference value of 3.2 eV for the anatase phase of nano-TiO₂ [53]. That structural changes occurred in the silica-coated samples is further demonstrated by the slight increase in E_g , which reflects changes in the material's optical and electrical properties, and possibly in its photocatalytic reactivity [54,55].

Table 2. Main features of TiO₂/SiO₂ spray-dried powder samples.

| Sample | SA _{BET} (m ² /g) | ζ-pot (mV) | E _g (eV) |
|--------------------------|---------------------------------------|------------|---------------------|
| TiO ₂ _15 | 154 | +43 ± 0.8 | 3.0 |
| TiO ₂ _21_Sil | 156 | +22 ± 0.3 | 3.2 |
| TiO ₂ _22_Sil | 175 | -15 ± 1.2 | 3.2 |
| SiO ₂ _2 | 174 | -34 ± 0.9 | nd* |

nd*: not determined

3.3 EPR analysis

EPR was used to measure ROS production by the pristine and silica-modified TiO₂. The data obtained were processed and compared, with (Fig. 5b) and without (Fig. 5a) normalizing to the content of TiO₂. The results showed that the silica-modified samples only produced fewer ROS by comparison with samples containing the same total amount of solid (titania and silica) (Fig. 5a). Otherwise, after normalizing to the TiO₂ content, the presence of silica increased ROS generation (Fig. 5b), as expected, given the reported capacity of silica coatings to improve the photoactivity of nano-TiO₂ surfaces [56-59]. There was no evidence of a very significant silica-dose-dependent trend in ROS production, however, as Figure 5b graphs clearly shows.

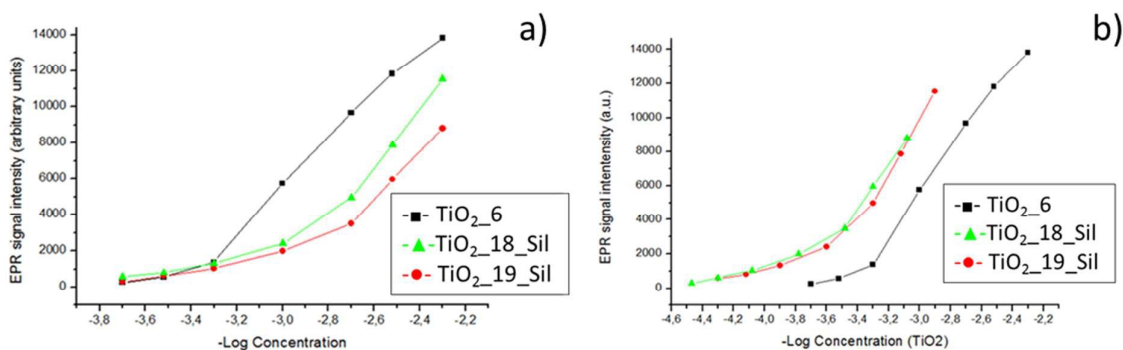


Figure 5. EPR signal as a function of: a) total solid concentration (TiO₂ and SiO₂), not normalized to TiO₂ content; and b) TiO₂ concentration, not normalized to TiO₂ content.

3.4 NO_x abatement test

The reactivity of untreated ceramic tiles was compared with that of pristine and silica-coated nano-TiO₂ samples to test the NO and NO_x abatement efficiency of the silica coating (Fig. 6). The inactivity of the support was demonstrated by a negligible reduction in the concentration detected vis-à-vis the untreated ceramic tile (Fig. 6a). Figures 6b and 6c show the expected improvement in the photocatalytic performance of the silica-encapsulated TiO₂ samples by comparison with the pristine sample. After 100 min, the NO abatement exceeded 90%, with a high conversion to NO₂, for both the silica-modified samples. It is worth noting that the silica-modified sample performed better than the pristine sample in

all cases when samples with the same total amount of TiO_2 (TiO_2_6 and $\text{TiO}_2_18_Sil$ sample) or the same total amount of solid ($\text{TiO}_2_37_Sil$ sample, with only 25% of the TiO_2 in the TiO_2_6 sample) were compared. Combined with the reduction in ROS detected for the silica-modified samples not normalized to the content of TiO_2 (Fig. 6a), this last result seems particularly promising as a SbD strategy. The desirable control of the structural alert relating to ROS production achieved by the presence of silica was unassociated with any negative fallout on photoactivity in the application considered, while it prompted an improvement in NO_x abatement capacity.

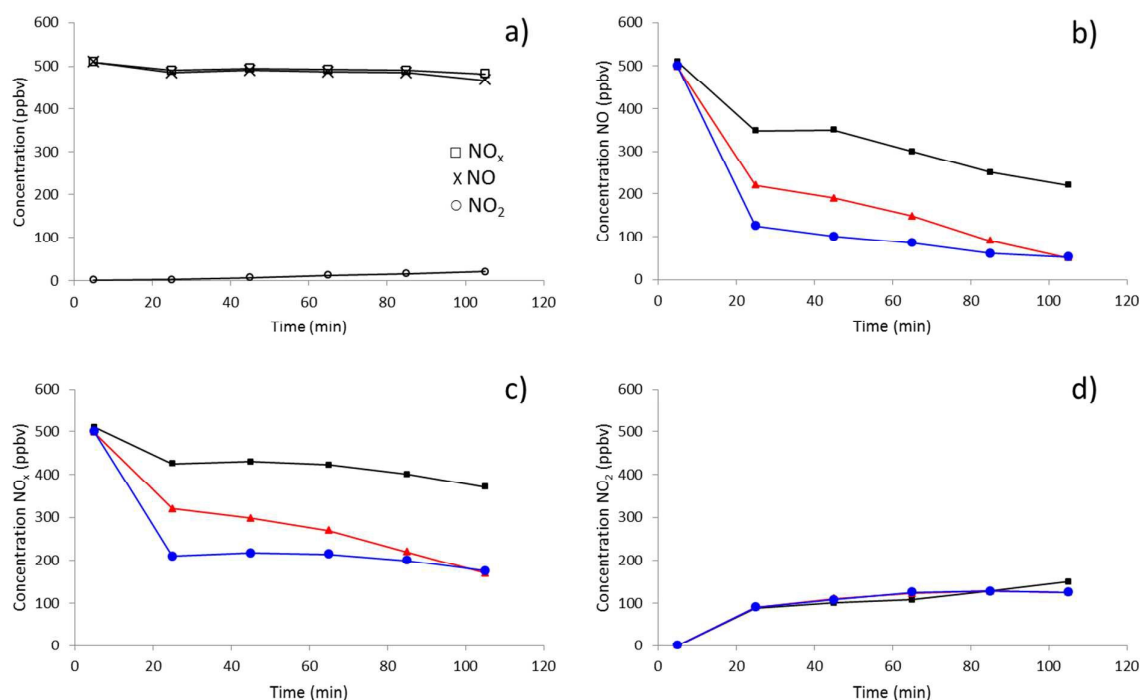


Figure 6. NO_x/NO abatement tests on: a) untreated, ■ TiO_2_6 -coated, ▲ $\text{TiO}_2_37_Sil$ -coated, and ● $\text{TiO}_2_18_Sil$ -coated ceramic tiles.

4. Conclusions

SiO_2 nanomatrices with encapsulated TiO_2 were obtained by means of a cost-effective and easily up-scalable colloidal heterocoagulation method that allowed for the NMs' surface to be engineered, preserving or improving their functional properties. Merging EPR results and DeNO_x activity data showed a higher NO_x/NO gas abatement and a lower ROS production in the silica-modified TiO_2 sample (not normalizing to the TiO_2 content). The value of adding silica to TiO_2 NPs was recognized by the decreased production of ROS, representing a positive response in terms of the reduction of potential hazard of this class of materials. From the industrial standpoint, the most interesting finding of the present study lies in that the presence of silica also improved the photocatalytic properties of the TiO_2 , and the abatement of NO_x , on samples normalized and not normalized to the content of TiO_2 . In addition to the ability of silica coating to

decrease the production of ROS, the result of performance tests encouraged the promotion of the present molecular design strategy also for the positive impact that the demonstrated possible use of a lower content of TiO₂ could have on the cost of the production process.

Acknowledgements

This research received support from the QNano Project (<http://www.qnano-ri.eu>) financed by the European Community Research Infrastructures under the FP7 Capacities Programme (Grant No. INFRA-2010-262163), and its partner (CRANN, Trinity College Dublin), and from the FP7 EU SANOWORK (Safe Nano Worker Exposure Scenarios) Collaborative Project (NMP4-SL-2012-280716). The authors also thank Valentina Dami (Colorobbia) and Mark Miller (IOM) for conducting the NO_x/NO abatement tests and EPR measurements, respectively.

References

- [1] A. Mills, S.K. Lee, *J. Photochem. Photobiol. A*, 2002, **152**, 233–247
- [2] A. Fujishima, T.N. Rao, D. Tryk, *J. Photochem. Photobiol. C: Photochem. Rev.*, 2000, **1**, 1–21
- [3] M. Langlet, A. Kim, M. Audier, J.-M. Herrmann, *J. Sol–Gel Sci. Technol.*, 2002, **25**, 223–234
- [4] R.I. Bickley, T. González-Carreno, J.S. Lees, L. Palmisano, R.J.D. Tilley, *J. Solid State Chem.*, 1991, **92**, 178–190
- [5] D.P. Macwan, P.N. Dave, S. Chaturvedi, *Mater. Sci.*, 2011, **46**, 3669–3686
- [6] S. Laufs, G. Burgeth, W. Duttlinger, R. Kurtenbach, M. Maban, C. Thomas, P. Wiesen, J. Kleffmann, *Atmospheric Environment*, 2010, **44**, 2341–2349
- [7] J. Ângelo, L. Andrade, A. Mendes, *Applied Catalysis A: General*, 2014, **484**, 17–25
- [8] A.M. Soylu, M. Polat, D. Altunoz Erdogan, Z. Say, C. Yildirim, Ö. Birer, E. Ozensoy, *Applied Surface Science*, 2014, **318**, 142–149
- [9] J. Shen, J. Liu, J. Ma, H. Zhang, X. Jiang, *Energy Conversion and Management*, 2015, **89**, 825–832
- [10] M. Pérez-Nicolás, J. Balbuena, M. Cruz-Yusta, L. Sánchez, I. Navarro-Blasco, J.M. Fernández, J.I. Alvarez, *Cement and Concrete Research*, 2015, **70**, 67–76
- [11] D.C. Carslaw, S.D. Beevers, M.C. Bell, *Atmospheric Environment*, 2007, **41**, 2073–2082
- [12] V. Stone, H. Johnston, M. J. D. Clift, *IEEE Trans. Nanobiosci.*, 2007, **6**, 331–340
- [13] Y. Ju-Nam, J. R. Lead, *Sci. Total Environ.*, 2008, **400**, 396–414
- [14] N. Li, T. Xia, A. E. Nel, *Free Radical Bio. Med.*, 2008, **44**, 1689–1699
- [15] H. J. Johnston, G. Hutchison, F. M. Christensen, S. Peters, S. Hankin, V. Stone, *Crit. Rev. Toxicol.*, 2010, **40**, 328–346

- [16] M. Valko, D. Leibfritz, J. Moncola, M. T.D. Cronin, M. Mazura, J. Telser, *Int. J. Biochem. Cell B.*, 2007, **39**, 44–84
- [17] S. George, H. Gardner, E.K. Seng, H.Chang, C.Y. Wang, C.H.Y. Fang, M. Richards, S. Valiyayeettil, W.K. Chan, *Environ. Sci. Technol.*, 2014, **48**, 6374–6382
- [18] G. Janer, E. Mas del Molino, E. Fernández-Rosas, A. Fernández, S. Vázquez-Campos, *Toxicol. Lett.*, 2014, **228**, 103–110
- [19] G. Morose, *J. Clean. Prod.*, 2010, **18**, 285–289
- [20] H. Zhang, D.R. Dunphy, X. Jiang, H. Meng, B. Sun, D. Tarn, M. Xue, X. Wang, S. Lin, Z. Ji, R. Li, F.L. Garcia, J. Yang, M.L. Kirk, T. Xia, J.I. Zink, A.E. Nel, C. Jeffrey, *J. Am. Chem. Soc.*, 2012, **134**, 15790–15804
- [21] B. Sun, Z. Ji, Y.-P. Liao, M. Wang, X. Wang, J. Dong, C. Hyun Chang, R. Li, H. Zhang, A.E. Nel, T. Xia, *ACS Nano*, 2013, **7**, 10834–10849
- [22] T. Xia, Y. Zhao, T. Sager, S. George, S. Pokhrel, N. Li, D. Schoenfeld, H. Meng, S. Lin, X. Wang, M. Wang, Z. Ji, J.I. Zink, L. Mädler, V. Castranova, S. Lin. A.E. Nel, *ACS Nano*, 2011, **5**, 1223–35
- [23] H. Zhang, S. Pokhrel, Z. Ji, H. Meng, X. Wang, S. Lin, C.H. Chang, L. Li, R. Li, B. Sun, M. Wang, Y.-P. Liao, R. Liu, T. Xia, L. Mädler, A.E. Nel, *J. Am. Chem. Soc.*, 2014, **136**, 6406–6420
- [24] S. George, S. Pokhrel, Z. Ji, B.L. Henderson, T. Xia, L. Li, J. I. Zink, A.E. Nel, L. Mädler, *J. Am. Chem. Soc.*, 2011, **133**, 11270–11278
- [25] B. Sun, S. Pokhrel, D.R. Dunphy, H. Zhang, Z. Ji, X. Wang, M. Wang, Y.-P. Liao, C. Hyun Chang, J. Dong, R. Li, L. Mädler, C. J. Brinker, A.E. Nel, T. Xia, *ACS Nano*, 2015, **9**, 9357–9372
- [26] X. Wang, T. Xia, M.C. Duch, Z. Ji, H. Zhang, R. Li, B. Sun, S. Lin, H. Meng, Y.-P. Liao, M. Wang, T.-B. Song, Y. Yang, M.C. Hersam, A.E. Nel, *Nano Lett.*, 2012, **12**, 3050–3061
- [27] R. Li, Z. Ji, C.H. Chang, D.R. Dunphy, X. Cai, H. Meng, H. Zhang, B. Sun, X. Wang, J. Dong, S. Lin, M. Wang, Y.-P. Liao, C.J. Brinker, A.E. Nel, T. Xia, *ACS Nano*, 2014, **8**, 1771–1783
- [28] R. Li, X. Wang, Z. Ji, B. Sun, H. Zhang, C.H. Chang, S. Lin, H. Meng, Y.-P. Liao, M. Wang, Z. Li, A.A. Hwang, T.-B. Song, R. Xu, Y. Yang, J.I. Zink, A.E. Nel, T. Xia, *ACS Nano*, 2013, **7**, 2352–2368
- [29] T. Xia, M. Kovoichich, M. Liong, J.I. Zink, A.E. Nel, *ACS Nano*, 2008, **2**, 85–96
- [30] K. Donaldson, A. Schinwald, F. Murphy, W.S. Cho, R. Duffin, L. Tran, C. Poland, *Account of chemical research*, 2013, **46**, 723–732
- [31] G. A. Sotiriou, C. Watson, K. M. Murdaugh, T. H. Darrah, G. Pyrgiotakis, A. Elder, J. D. Brain, P. Demokritou, *Environ. Sci.: Nano*, 2014, **1**, 144-153

- [32] M.A. Malvindi, V. De Matteis, A. Galeone, V. Brunetti, G. C. Anyfantis, A. Athanassiou, R. Cingolani, P.P. Pompa, *PLoS ONE*, 2014, **1**, e85835
- [33] J. Ma, R. R. Mercer, M. Barger, D. Schwegler-Berry, J. M. Cohen, P. Demokritou, V. Castranova, *Toxicology and Applied Pharmacology*, 2015, **288**, 63–73
- [34] R. K. Singh, T.-H. Kim, K. D. Patel, J. C. Knowles, H.-W. Kim, *J. Biomed. Mater. Res. A*, 2012, **100**, 1734–1742
- [35] M. Okubo, Y. He, K. Ichikawa, *Colloid. Polym. Sci.*, 1991, **269**, 125–130
- [36] G. Li, X. Yang, J. Wang, *Colloids and Surfaces A: Physicochem. Eng. Aspects*, 2008, **322**, 192–198
- [37] K. Yamaguchi, M. Ito, T. Taniguchi, S. Kawaguchi, K. Nagai, *Colloid. Polym. Sci.*, 2004, **282**, 366–372
- [38] D. Gardini, M. Blosi, C. Delpivo, S. Ortelli, A.L. Costa, *J. Phys. Conf. Ser.*, 2013, **429**, 012052
- [39] S. Lu, R. Duffin, C. Poland, P. Daly, F. Murphy, E. Drost, W. MacNee, V. Stone, K. Donaldson, *Environmental Health Perspectives*, 2009, **117**, 241–247
- [40] R. F. Howe, M. Gratzel, *J. Phys. Chem.*, 1985, **89**, 4495–4499
- [41] R. F. Howe, M. Gratzel, *J. Phys. Chem.*, 1987, **91**, 3906–3909
- [42] S. Ortelli, M. Blosi, C. Delpivo, D. Gardini, M. Dondi, I. Gualandi, D. Tonelli, V. Aina, I. Fenoglio, A. Gandhi, S. Tofail, A.L. Costa, *J. Photochem. Photobiol. A: Chem.*, 2014, **292**, 26–33
- [43] R. López, R. Gómez, *J. Sol–Gel Sci. Technol.*, 2012, **61**, 1–7
- [44] J. Li, Y. Cai Zhang, M. Zhang, *Mater. Lett.*, 2012, **79**, 136–138
- [45] G. Bartosz, *Clinica Chimica Acta*, 2006, **368**, 53–76
- [46] S. Marklund, G. Marklund, *Eur. J. Biochem.*, 1974, **47**, 469–474
- [47] M. Miller, S. Borthwick, C. Shaw, S. McLean, D. McClure, N. Mills, R. Duffin, K. Donaldson, I. Megson, P. Hadoke and D. Newby, *Environmental Health Perspectives*, 2009, **117**, 611–616
- [48] Q. Wu, Z. Wang, X. Kong, X. Gu, G. Xue, *Langmuir*, 2008, **24**, 7778–7784
- [49] J. Sun, L. Gao, *Carbon*, 2003, **41**, 1063–1068
- [50] N.J. Zuidam, V.A. Nedović, *Encapsulation Technologies for Active Food Ingredients and Food Processing*, Springer Science+Business Media, LLC, 2010
- [51] S. Ortelli, A.L. Costa, Nanoencapsulation techniques as useful tool towards "safer by molecular design", accepted to *Nano-Structures & Nano-Objects*
- [52] D. Y. Kong, M. Yu, C. K. Lin, X. M. Liu, J. Lin, J. Fang, *Journal of The Electrochemical Society*, 2005, **152**, H146–H151
- [53] X. Wang, H. Hu, Z. Yang, Y. Kong, B. Fei, J.H. Xin, *Catalysis Communications*, 2015, **72**, 81–85
- [54] Y. Zhao, C. Li, X. Liu, F. Gu, H. Jiang, W. Shao, L. Zhang, Y. He, *Materials Letters*, 2007, **61**, 79–83

- [55] K. Madhusudan Reddy, Sunkara V. Manorama, A. Ramachandra Reddy, *Materials Chemistry and Physics*, 2002, **78**, 239–245
- [56] C. Anderson, A.J. Bard, *J. Phys. Chem. B*, 1997, **101**, 2611–2616
- [57] K.Y. Jung, S.B. Park, *J. Photochem. Photobiol. A: Chem.*, 1999, **127**, 117–122
- [58] T. Yuranova, R. Mosteo, J. Bandara, D. Laub, J. Kiwi, *J. Mol. Catal. A: Chem.*, 2006, **244**, 160–167
- [59] E. Pakdel, W.A. Daoud, *J. Colloid Interface Sci.*, 2013, **401**, 1–7

Environmental Science nano

Nano Impact statement:

The paper aims to provide a surface engineering solution for the control of TiO₂ nanoparticles risk determinant properties: size, morphology, production of reactive oxygen species (ROS), photocatalytic performances. The paper represents one of the first attempts to find a correlation between surface engineering strategy (silica matrix encapsulation) and one risk determinant property for redox reactive species (as for instance nano TiO₂) such as the reactive oxygen species (ROS) production. Silica matrix encapsulation actually controls the emission of ROS, but improves the photocatalytic performance tested within ceramic tile nanostructured coating. The approach can be generalized to other semiconductor based nanoparticles, representing a possible “safety by molecular design strategy” for nanomaterial risk management. The nano impact is strong because the results promote safety by design as a friendly and sustainable primary prevention approach to nanomaterial risk management.